

# JGR Atmospheres

## RESEARCH ARTICLE

10.1029/2019JD030558

### Key Points:

- Smoke significantly impacts meteorological conditions near wildland fires by radiatively driven near-surface cooling and warming aloft
- Positive feedback is observed, where increasing smoke concentrations enhance atmospheric stability, reduce mixing, and increase near-surface PM<sub>2.5</sub> concentrations
- Radiative effects of wildfire smoke can be simulated in an integrated framework coupling atmospheric, fire, and chemical transport models

### Correspondence to:

A. K. Kochanski,  
adam.kochanski@utah.edu

### Citation:

Kochanski, A. K., Mallia, D. V., Fearon, M. G., Mandel, J., Sour, A. H., & Brown, T. (2019). Modeling wildfire smoke feedback mechanisms using a coupled fire-atmosphere model with a radiatively active aerosol scheme. *Journal of Geophysical Research: Atmospheres*, 124, 9099–9116. <https://doi.org/10.1029/2019JD030558>

Received 27 FEB 2019

Accepted 29 JUN 2019

Accepted article online 12 JUL 2019

Published online 22 AUG 2019

### Author Contributions:

**Conceptualization:** Adam K.

Kochanski, Matthew G. Fearon, Amir H. Sour, Tim Brown

**Formal analysis:** Adam K. Kochanski, Derek V. Mallia, Matthew G. Fearon, Amir H. Sour, Tim Brown

**Funding acquisition:** Adam K. Kochanski, Tim Brown

**Investigation:** Adam K. Kochanski, Derek V. Mallia, Amir H. Sour, Tim Brown





**Methodology:** Adam K. Kochanski, Derek V. Mallia, Amir H. Sour, Tim Brown

**Project administration:** Adam K. Kochanski, Tim Brown

**Resources:** Adam K. Kochanski, Jan Mandel, Tim Brown

**Software:** Jan Mandel  
(continued)

## Modeling Wildfire Smoke Feedback Mechanisms Using a Coupled Fire-Atmosphere Model With a Radiatively Active Aerosol Scheme

Adam K. Kochanski<sup>1</sup> , Derek V. Mallia<sup>1</sup>, Matthew G. Fearon<sup>2</sup> , Jan Mandel<sup>3</sup> , Amir H. Sour<sup>4</sup> , and Tim Brown<sup>2</sup>

<sup>1</sup>Department of Atmospheric Sciences, University of Utah, Salt Lake City, UT, USA, <sup>2</sup>Desert Research Institute, Reno, NV, USA, <sup>3</sup>Department of Mathematical and Statistical Sciences, University of Colorado Denver, Denver, CO, USA,

<sup>4</sup>Harvard-Smithsonian Center for Astrophysics, Cambridge, MA, USA

**Abstract** During the summer of 2015, a number of large wildfires burned across Northern California in areas of localized topographic relief. Persistent valley smoke hindered fire-fighting efforts, delayed helicopter operations, and exposed communities to extreme concentrations of particulate matter. It was hypothesized that smoke from the wildfires reduced the amount of incoming solar radiation reaching the ground, which resulted in near-surface cooling, while smoke aerosols resulted in warming aloft. As a result of increased inversion-like conditions, smoke from wildfires was trapped within mountain valleys adjacent to active wildfires. In this study, wildfire smoke-induced inversion episodes across Northern California were examined using a modeling framework that couples an atmospheric, chemical, and fire spread model. Modeling results examined in this study indicate that wildfire smoke reduced incoming solar radiation during the afternoon, which led to local surface cooling by up to 3 °C, which agrees with cooling observed at nearby surface stations. Direct heating from the fire itself did not significantly enhance atmospheric stability. However, midlevel warming (+0.5 °C) and pronounced surface cooling was observed in the smoke layer, indicating that smoke aerosols significantly enhanced atmospheric stability. A positive feedback associated with the presence of smoke was observed, where local smoke-enhanced inversions inhibited the growth of the planetary boundary layer, and reduced surface winds, which resulted in smoke accumulation that further reduced near-surface temperatures. This work suggests that the inclusion of fire-smoke-atmosphere feedback in a coupled modeling framework such as WRF-SFIRE-CHEM can forecast the dispersion of wildfire smoke and its radiative feedback, and potentially provide decision-support for wildfire operations.

## 1. Introduction

Wildfires are responsible for emitting large quantities of smoke, which can have significant impacts on air quality (Ignotti et al., 2010), radiative fluxes (Robock, 1988; Stone et al., 2011; Yu et al., 2016), visibility (Achtemeier, 2009), and cloud microphysics (Kaufman & Nakajima, 1993). Smoke from wildfires can also promote daytime surface cooling by blocking sunlight (Robock, 1988). Aerosols from wildfires consist of a wide spectrum of absorptive and scattering particles, mostly in the form of organic and black carbon, respectively. Since black and organic carbon have different optical properties, the interactions of smoke with solar radiation can be complex (Colbeck et al., 1997).

Robock (1991) found that wildfire smoke cooled daytime surface temperatures by 1.5 to 7 °C within mountain valleys across Northern California. Another study by Youn et al. (2011) found that smoke emitted from Siberian fires resulted in temperature decreases of 3.5 °C across the region with surface pressure anomalies of +5.6 hPa. The cooling effect of wildfire smoke is associated with presence of aerosols modifying the Earth's radiative budget by scattering and absorption of incoming solar radiation. This effect, which is often referred to as *smoke shading*, can reduce afternoon near-surface temperatures if there is sufficient aerosol loading in the atmosphere to decrease downwelling shortwave radiation via absorption and scattering (Lareau & Clements, 2015; Robock, 1988, 1991). Smoke shading can suppress convective boundary layer growth, which can result in persistent near-surface temperature inversions that inhibit the dispersion of smoke (Garrett et al., 1990; Robock, 1988; Segal et al., 1989).

It has been hypothesized that wildfire smoke can cause a positive feedback where additional smoke aerosols accumulate as a result of slower smoke dispersion, which can further amplify the near-surface temperature

**Supervision:** Adam K. Kochanski, Tim Brown

**Validation:** Derek V. Mallia, Matthew G. Fearon

**Visualization:** Adam K. Kochanski, Derek V. Mallia

**Writing - original draft:** Adam K. Kochanski, Derek V. Mallia

**Writing - review & editing:** Adam K. Kochanski, Derek V. Mallia, Matthew G. Fearon, Amir H. Souri, Tim Brown

inversion due to increased absorption and scattering of downwelling solar radiation (Robock, 1991). Persistent smoke-induced inversions most often occur in areas of significant topographic relief (e.g., mountain valleys), which can trap smoke aerosols resulting in inversions that can persist for several weeks. Interactions between the aerosols and the boundary layer process have been extensively studied over past years (Li et al., 2017). However, much of the existing literature has only focused on aerosol-boundary layer interactions at the regional and global scales, usually with an emphasis on urban air quality.

Smoke-induced inversions can also have significant impacts on people by exposing the affected population to prolonged periods of degraded air quality as a result of hazardous concentrations of particulate matter (e.g.,  $PM_{2.5}$ ). High concentrations of  $PM_{2.5}$  often have adverse effects on human health, as inhaled particulates can penetrate deep into people's lungs (Huttunen et al., 2012; Johnston et al., 2012; Zelikoff et al., 2002). Smoke inversions can also impair visibility, presenting a challenge for transportation and fire management operations (Goodrick et al., 2012).

Wildfire smoke poses a significant hazard to communities and fire management. Thus, the ability to predict fire-atmosphere feedback such as smoke-induced inversions would benefit air quality and fire management personnel. In addition, wildfire activity is projected to increase through the end of twenty-first century as a result of climate change (Spracklen et al., 2009). Thus, improving the understanding of fire-atmosphere feedback and developing better forecast tools that can account for fire-atmosphere interactions will become increasingly important. Despite advancements in numerical weather prediction (NWP) models, forecasting smoke and smoke dispersion remains challenging due to uncertainties associated with fire emissions, fuel characteristics, vertical smoke distribution, and fire-atmosphere interactions (Goodrick et al., 2012; Larkin et al., 2009; Mallia et al., 2018; Val Martin et al., 2012). Furthermore, operational NWP models generally do not account for fire-atmosphere interactions and often neglect radiative effects from aerosols, thus are unable to resolve smoke-induced inversions (Lareau & Clements, 2015).

Recently, a coupled fire-atmosphere model (WRF-SFIRE; Mandel et al., 2011) was integrated with a chemical model (WRF-SFIRE-CHEM; Kochanski et al., 2016) in an effort to simultaneously simulate fire spread, fire plume rise, smoke dispersion, and plume chemistry. In addition, this modeling framework has the ability to simulate radiative feedback associated with smoke aerosols; however, this capability has not been thoroughly tested. Here the WRF-SFIRE-CHEM framework was applied to a case study where significant wildfire smoke was observed, which potentially resulted in cooler surface temperatures and persistent inversions.

During the summer of 2015, a number of large wildfires burned across Northern California in areas of localized topographic relief (Figure 1). Persistent valley smoke hindered fire-fighting efforts, delayed helicopter operations, and exposed communities to high concentrations of atmospheric pollutants. While nighttime inversion conditions are typical in valleys across the western United States, the inversion during this event lasted longer than usual, as it persisted through the late afternoon on 19 August 2015. According to surface meteorological stations, pronounced cooling was observed within valleys across Northern California, while upper elevation locations above the smoke layer saw minimal decreases in surface temperatures. It was hypothesized that the combination of increased scattering and absorption within the smoke layer and midlevel atmospheric heating from the fire stabilized the atmosphere and extended the inversion period.

The study presented here will focus on the local meteorological effects of wildland fire smoke, which can be important to understand for firefighting operations and air quality management. While previous modeling studies investigated relatively homogeneous well-mixed aerosol layers, the work presented here represents the first modeling effort focused on the small-scale processes associated with fire-atmosphere interactions typically neglected in air quality models, which treat fire emissions as point sources with no exchange of fire heat to the atmospheric model. For this study, aerosol effects are modeled simultaneously with fire progression, emissions, plume rise, and fuel moisture evolution using an integrated modeling system.

In the following sections, we will first describe the model setup, which was used to investigate and quantify the radiative impacts of smoke aerosols on mountain valley inversions (section 2.1) along with a brief description on the observations used to verify simulated results (section 2.2). A basic description of the case study investigated for this study is presented in section 3. Results and conclusions for this work are presented in sections 4 and 5, respectively.

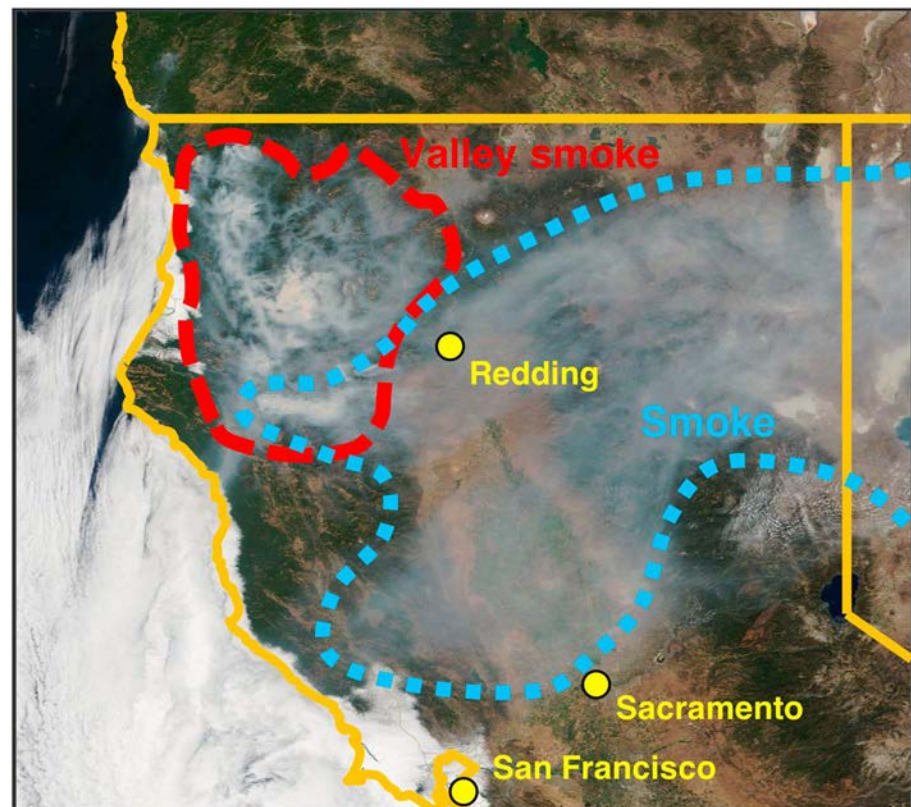


**Figure 1.** True color satellite image from MODIS (Terra) of wildfire smoke across Northern California on 20 August 2015. The red-dashed line indicated smoke trapped within valleys across Northern California, while the light blue-dashed line outlines the general smoke plume.

## 2. Methodology

### 2.1. Modeling Framework

The WRF-SFIRE-CHEM modeling framework (WRFSC), which couples a fire-atmosphere model with a chemical transport model (WRF-CHEM; Grell & Baklanov, 2011), was used to simulate smoke-induced inversions observed across Northern California on 19–20 August 2015. The integration of the atmospheric, fire, and chemical transport models enables WRFSC to explicitly simulate the fire propagation, plume rise, and smoke dispersion and chemistry (Kochanski et al., 2016). For the purpose of this study, WRFSC's integration with the RADM2 (Stockwell et al., 1990) and MOZART (Emmons et al., 2010) chemical mechanisms was extended to the Goddard Chemistry Aerosol Radiation and Transport (GOCART) scheme (Chin et al., 2000). In this setup, the fuel consumption computed by the fire component of the system is converted into the fluxes of  $\text{SO}_2$ ,  $\text{PM}_{2.5}$ , organic carbon, black carbon, and  $\text{PM}_{10}$ . Emissions are then injected into the first model layer and are transported by model-resolved pyroconvection and advection. WRFSC's integration with the GOCART scheme has been implemented to enable aerosol interactions with incoming solar radiation at a modest computational cost, which is often necessary for forecasting applications. A schematic diagram showing the coupling mechanisms between WRFSC components can be seen in Figure 2. The WRFSC code used in this study, which is based on WRF v3.4.1, is publicly available at the Open Wildland Fire Modeling repository under <http://github.com/openwfm/wrf-fire/>.

WRFSC has been configured with three nested domains with grid spacing of 12, 4, and 1.33 km, respectively. A total of six fires were simulated, with five of them being located within the innermost domain (d03) and one within the 4-km domain (d02; Figure 3). WRFSC simulations were initialized on 16 August 0000 UTC and run for seven days, with boundary conditions coming from the Climate Forecast System Reanalysis (Saha et al., 2014). The fire component of the system computing fuel consumption and emissions was executed on a 1:20 refined mesh, with a horizontal resolution of 67 m in d03 and 200 m in d02.

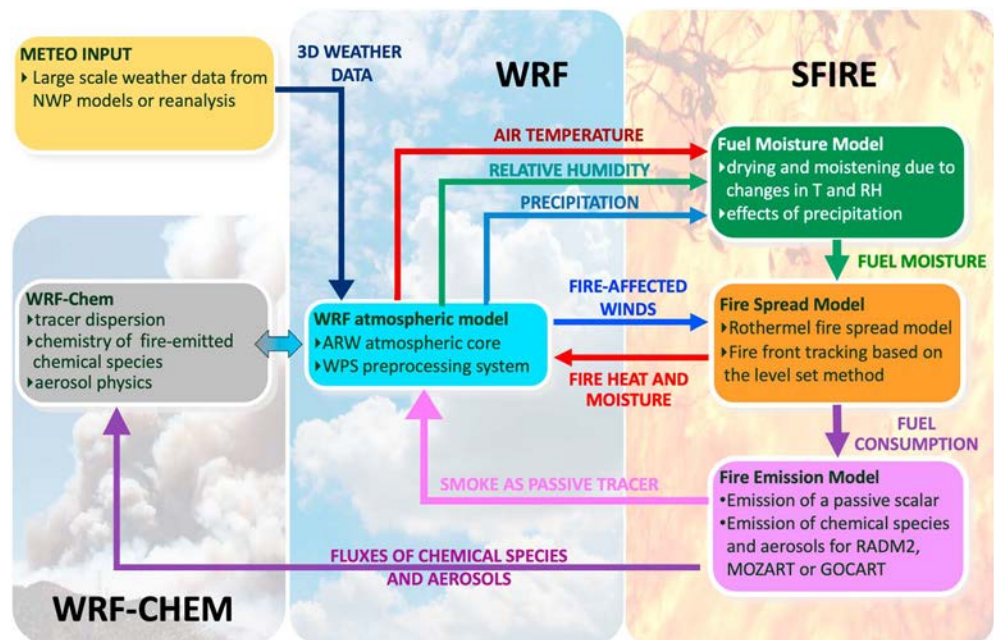


**Figure 2.** Diagram of the data flow in the WRF-SFIRE-CHEM (WRFSC) model used in this study.

LANDFIRE was used to provide WRFSC with high-resolution fuel descriptions and elevation data (<https://www.landfire.gov/>). The fuel moisture model (Vejmelka et al., 2015) was initialized uniformly across the computational domain based on the National Fuel Moisture Database data available on the Wildland Fire Assessment System (<http://www.wfas.net/>), and was run in-line with the atmospheric model. This model provides fuel moisture estimates, which are used for the fire spread computation within the WRFSC forecast runs. The initial fuel moisture values as well as the detailed WRF configuration are presented in Table 1.

### 2.1.1. Sensitivity Simulations

Three numerical simulations were carried out in order to quantify the impacts of wildland fires and smoke on vertical temperature profiles in valleys adjacent to actively burning fires across Northern California. The first simulation (1) was performed under no-fire and no-smoke conditions. This configuration was intended to serve as a proxy for a generic atmospheric simulation, which neglects the atmospheric impacts of fire and smoke. The second simulation (2), defined as the “baseline simulation,” was run with WRFSC utilizing coupling between fire emissions and the GOCART aerosol scheme, but with the radiative smoke impacts turned off. In this simulation, fire heat and emission fluxes were injected into the atmosphere, but smoke was

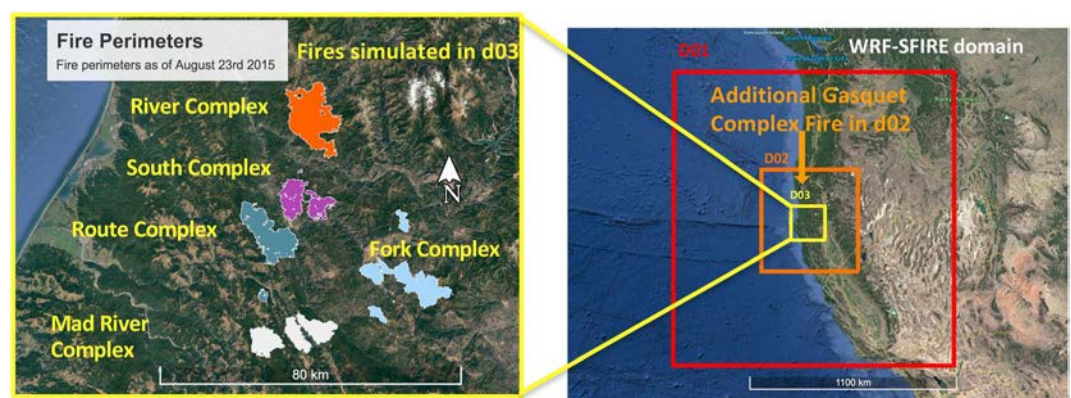


**Figure 3.** (left) Active fires across Northern California on 23 August 2015 within the innermost domain d03 and (right) the model domain setup with the indication of the additional fire within domain d02.

**Table 1**  
Detailed WRF Configuration Used in the Study

Domains	d01	d02	d03
Horizontal resolution of atmospheric model	12 km	4 km	1.33 km
Horizontal resolution of the fire model	-	200 m	67.7 m
Number of grid points ( $x \times y \times z$ )	$130 \times 130 \times 41$	$130 \times 130 \times 41$	$130 \times 130 \times 41$
Initial 1-hr fuel moisture	-	4.4%	4.4%
Initial 10-hr fuel moisture	-	10%	10%
Initial 100-hr fuel moisture	-	12.2%	12.2%
Initial life fuel moisture	-	86%	86%
Time step	18 s	6 s	2 s
Microphysics	Lin et al. <sup>a</sup>	Lin et al. <sup>a</sup>	Lin et al. <sup>a</sup>
PBL physics	YSU <sup>b</sup>	YSU <sup>b</sup>	YSU <sup>b</sup>
Surface model	Noah <sup>c</sup>	Noah <sup>c</sup>	Noah <sup>c</sup>
Cumulus parameterization	Grell-Devenyi <sup>d</sup>	Grell-Devenyi <sup>d</sup>	-
Chemical option	300	300	300

<sup>a</sup>Chen and Sun (2002). <sup>b</sup>Hong et al. (2006). <sup>c</sup>Tewari et al. (2004).

<sup>d</sup>Grell and Devenyi (2002).

instead of being constrained by observed fire perimeters (simulations described in section 2.2). This configuration was used to test the feasibility of running WRFSC in an operational setting where fire growth would be driven by meteorology, fuel characteristics, and topography instead of being constrained by fire perimeters, which are generally not available in a forecast setting. This approach is fundamentally different from what is used in the current operational systems such as BlueSky (Larkin et al., 2009) or HRRR-smoke (Ahmadov et al., 2017), which estimate future emissions based on the last day fire activity (i.e., persistence). Forecast simulations were initialized on 18 August at 1200 UTC, after spinning up for 48 hr. For the first 48

treated as being radiatively inactive. The third simulation (3) utilized a similar model configuration as the second setup, where smoke emissions computed from fuel consumption were linked to the GOCART aerosol scheme. However, in this setup, smoke aerosols were allowed to interact with the Rapid Radiative Transfer Model for GCMs (Iacono et al., 2008). The fuel-specific emission factors for PM<sub>2.5</sub>, OC, and BC were obtained from Urbanski (2014) and Akagi et al. (2011). In this configuration, WRFSC rendered both the thermodynamic impact of fire heat as well as the radiative impacts of smoke aerosols on incoming solar radiation.

For the three configurations described above, fire growth was constrained using airborne infrared perimeters available on the Geospatial Multi-Agency Coordination (GeoMAC) website (<https://rmgsc.cr.usgs.gov/outgoing/GeoMAC/>) operated by the U.S. Department of the Interior and the U.S. Department of Agriculture. The fire propagation history was encoded as a fire arrival time, which was derived by spatially interpolating daily fire perimeters. The results from this set of hindcast simulations (hereafter, “constrained runs”) are discussed in sections 4.1–4.3.

### 2.1.2. Forecast Simulation With Dynamic Fire Progression

An additional set of simulations were carried out using a “forecast configuration,” where the fire growth was driven by simulated weather conditions, fuel moisture, fuel type, and topography (i.e., fully coupled), instead of being constrained by observed fire perimeters (simulations described in section 2.2). This configuration was used to test the feasibility of running WRFSC in an operational setting where fire growth would be driven by meteorology, fuel characteristics, and topography instead of being constrained by fire perimeters, which are generally not available in a forecast setting. This approach is fundamentally different from what is used in the current operational systems such as BlueSky (Larkin et al., 2009) or HRRR-smoke (Ahmadov et al., 2017), which estimate future emissions based on the last day fire activity (i.e., persistence). Forecast simulations were initialized on 18 August at 1200 UTC, after spinning up for 48 hr. For the first 48 hr prior to 18 August, the fire progression was driven by the fire history derived from fire perimeters, similar to the hindcast runs described in the previous section. This spin-up period was intended to ensure that a realistic large-scale smoke distribution and fuel moisture were established prior to the start of the forecast run. The fire initialization included two steps: removing the fuel from grid cells burnt prior to the simulation start, followed by prescribing initial fire progression from the perimeter-derived fire arrival time. After 48 hr of model spin-up, the fire progression was driven by fuel characteristics and meteorology in a fully two-way coupled mode for the next 96 hr. Results from this run are presented in section 4.4.

## 2.2. Observations

### 2.2.1. Portable PM<sub>2.5</sub> Stations

A number of portable PM<sub>2.5</sub> stations were deployed across Northern California during the summer of 2015, courtesy of the Western Region Climate Center and the Interagency Real-Time Smoke Monitoring (AIRSIS) systems. These portable stations were deployed as part of the Wildland Fire Air Quality Response Program (<https://wildlandfires-moke.net>). Five of these stations were located in valleys that were adjacent to the wildfires of interest (Figure 4). To measure PM<sub>2.5</sub>, these stations were either outfitted with an E-Sampler or an E-BAM measurement instrument, which were both manufactured by Met One Inc. PM<sub>2.5</sub> concentrations measured at these sites were used to validate predicted wild-fire smoke concentrations within WRFSC (see Tables 2 and 3).

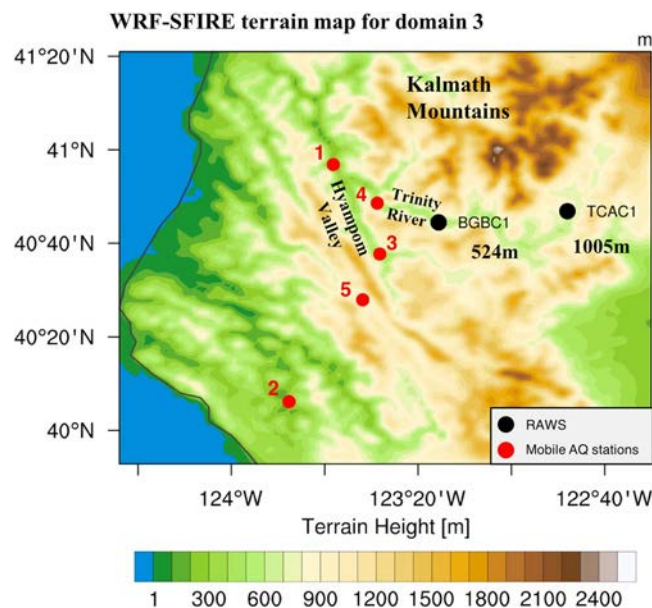


**Figure 4.** Terrain map of the innermost model domain (d03). BGBC1 is the Big Bar station located toward the bottom of the Trinity River valley (elevation of 524 m), while TCAC1 denotes the Trinity Camp observation site, located at the top of the Trinity River valley (elevation of 1,005 m). Red circles represent locations of mobile air quality stations.

**Table 2**  
*Average Modeled and Observed PM<sub>2.5</sub> Concentrations ( $\mu\text{g}/\text{m}^3$ )*

	Mean observation	Mean model	Bias	Relative bias
Station 1	177.0	142.8	−34.2	−19%
Station 2	23.5	31.8	8.3	35%
Station 3	496.3	1047.2	550.9	111%
Station 4	315.0	293.2	−21.8	−7%
Station 5	99.9	100.4	0.5	1%

<sup>a</sup>Mean concentrations were averaged between 17 and 22 August 2015.

### 2.2.2. Plume Top Height Data (Multi-angle Imaging SpectroRadiometer)

The Multi-angle Imaging SpectroRadiometer (MISR) and Moderate Resolution Imaging Spectroradiometer data were used to retrieve the plume top heights for the fires across Northern California during the time of interest. MISR provides stereoscopic imaging capability with 275-m spatial resolution for 672-nm spectral band and 1.1-km spatial resolution for 446-nm spectral band, which can be combined with Moderate Resolution Imaging Spectroradiometer thermal anomalies to identify fires and estimate fire plume top heights. Wildfire plumes

within the domain and time of interest (18 August at 1900 UTC) were digitized and processed using the MISR Interactive eXplorer (MINX) v.4 (Nelson, Averill, et al., 2008, Nelson, Chen, et al., 2008, Nelson et al., 2013).

## 3. Case Description

Throughout the month of August, daytime inversion conditions were observed across Northern California. It was hypothesized that smoke originated from six large wildfires that were actively burning across Northern California during this time (Figure 3). The most severe smoke conditions were observed during the afternoon of 19 August 2015. Here smoke was responsible for impacting fire-fighting efforts, grounding helicopter operations, and degrading air quality across the region. Smoke was particularly thick south of the Kalmath Mountains, which resulted in a significant decrease in 2-m temperature at a meteorological station located toward the bottom of Trinity River Valley (see Figure 4). The lack of cloud cover across the study domain during the days of most pronounced surface cooling made this episode ideal for analyzing the radiative impacts of smoke.

Incoming solar radiation and temperature from both WRF-SFIRE model configurations were compared to observations at two stations that were adjacent to the River Complex and South Complex fires. The first station (Big Bar; BGBC1) was located within the Trinity River valley (elevation = 524 m), while the second site (Trinity Camp; TCAC1) was located at the top of the Trinity River Valley with an elevation of 1,005 m. The elevation map of the innermost model domain and the location of these two stations are shown in Figure 4.

BGBC1, located deeper within the Trinity River Valley relative to TCAC1, observed a much larger decrease in incoming solar radiation on 19 August when compared to TCAC1 (Figure 5), as well as a larger temperature decrease (see section 4). The gradual breakdown of the 500-hPa ridge centered across western United States was likely partially responsible for the cooler daytime temperatures (Figure 6). However, the large decreases in incoming solar radiation seen in Figure 5 at BGBC1 suggest that synoptic-scale cooling was not the only factor behind the temperature decreases observed at BGBC1. Based on the geographic locations of these stations, it was hypothesized that the temperature and solar radiation differences observed at BGBC1 and TCAC1 were the result of different site elevations. BGBC1, which was located deeper in the valley, likely had a larger aerosol optical depth (thicker smoke layer) relative to TCAC1, which was located higher in the mountains.

## 4. Results

### 4.1. Basic Validation of the Plume Rise and Surface PM<sub>2.5</sub> From the Hindcast Simulation

The ability for NWP models to realistically represent the vertical plume distribution is critical from the standpoint of smoke dispersion, and smoke radiative impacts (Liu et al., 2008; Mallia et al., 2018; Walter et al., 2016). This task can be particularly challenging for coupled fire-atmosphere models, which must simultaneously resolve pyroconvection and fire growth. In order to assure that the WRFSC simulations were able to grid spacing plume development, simulated plume top heights were compared to derived plume tops from MISR.

**Table 3**  
*Average Forecast and Observed PM<sub>2.5</sub> Concentrations ( $\mu\text{g}/\text{m}^3$ )*

	Mean observation	Mean model	Bias	Relative bias
Station 1	176.8	161.4	−15.6	−9%
Station 2	23.5	33.3	9.8	42%
Station 3	496.3	1281.9	785.6	158%
Station 4	315.2	407.7	92.7	29%
Station 5	99.9	126.8	26.8	27%

<sup>a</sup>Mean concentrations were averaged between 17 and 22 August 2015.

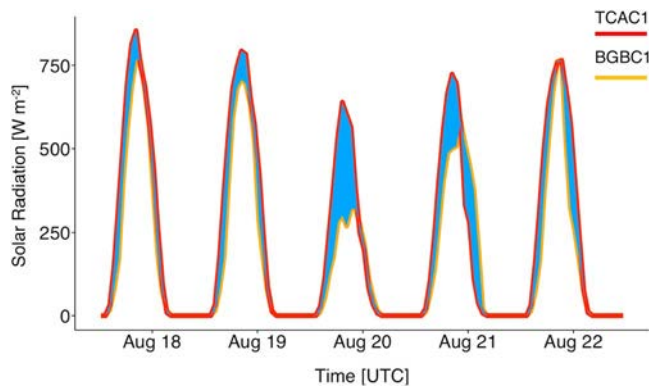


**Figure 5.** Time series of observed incoming solar radiation at BGBC1 and TCAC1 stations. The light blue shading highlights differences in the solar radiation measured at these sites.

Overall, the hindcast WRFSC simulation was able to realistically capture the vertical extent of the smoke plume (Figure 7). The histograms presented in Figures 7a and 7c indicate good agreement between the observed (2,240 m above sea level) and simulated (2,306 m above sea level) mean plume top height on 18 August 18 at 1900 UTC. Figures 7b and 7d indicate that the overall plume orientation was also captured correctly by each model configuration. However, it is important to note that MISR was only able to provide a single estimate of the vertical extent of a dynamically evolving plume as satellite overpasses over a single area are infrequent. Despite the lack of observations, WRFSC simulations did indicate that fire plume heights continued to increase throughout the afternoon from 2,000 to 2,800 m above ground level despite the presence of increased stability from aerosol feedbacks. Finally, it is worth noting that there are a number of points where MISR reported missing data, likely due to the sensor's inability to detect thin smoke plume, and smoke over mountaintops and oceans (Figure 7a).

Simulated  $PM_{2.5}$  concentrations from the hindcast model runs were also validated against observations obtained from air quality stations deployed during Wildland Fire Air Quality Response Program. Simulated and observed  $PM_{2.5}$  were averaged between 17–22 August 2015 (Table 2). Results here suggest that simulated  $PM_{2.5}$  was in agreement with observed concentrations. The spatial variability of  $PM_{2.5}$  across the region was well captured by the model with the lowest and highest concentrations being reported at stations 2 and 3, respectively (Table 2). However, modeled concentrations at station 3, which was located

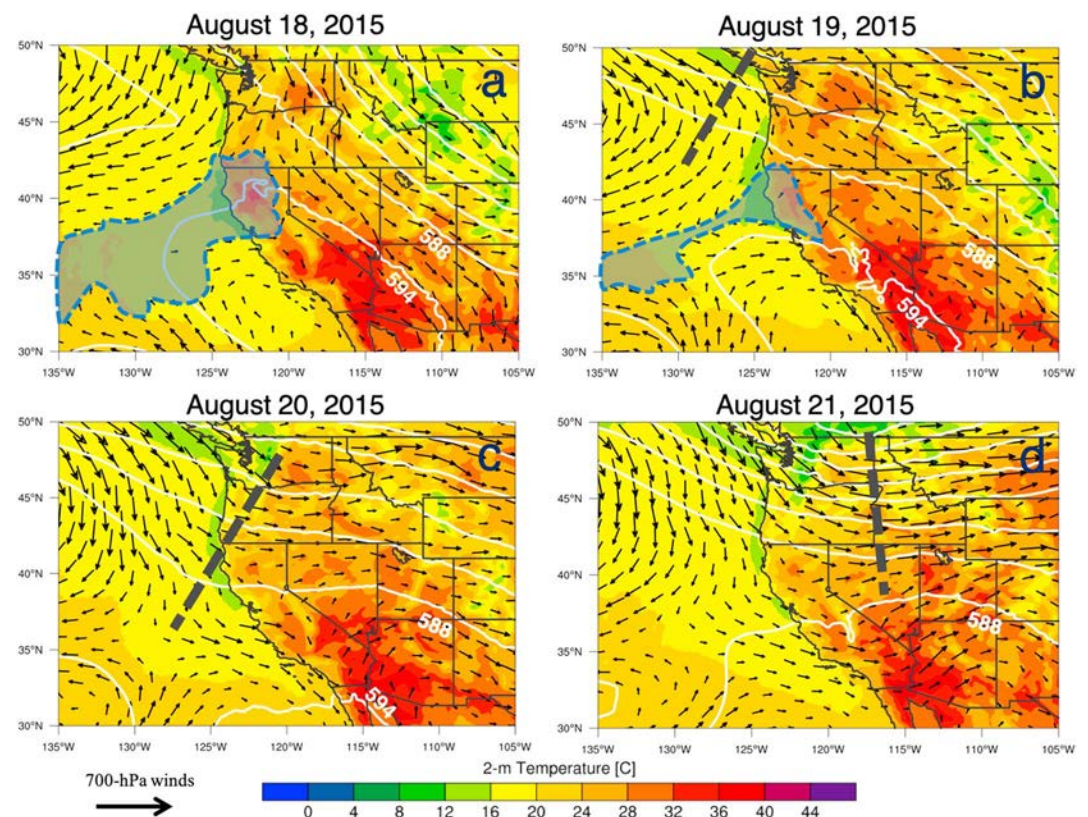


**Figure 6.** Synoptic-scale conditions for the western United States at 18:00 UTC on (a) 18 August, (b) 19 August, (c) 20 August, and (d) 21 August. Color-filled contours represents 2-m temperature ( $^{\circ}\text{C}$ ), white lines indicate 500-hPa geopotential heights contoured every 6 dam, and the black vectors indicate 700-hPa winds (m/s) greater than 3 m/s. Blue shaded area indicates regions with winds less than 3 m/s and the black-dashed line represents the axis of the short-wave trough.

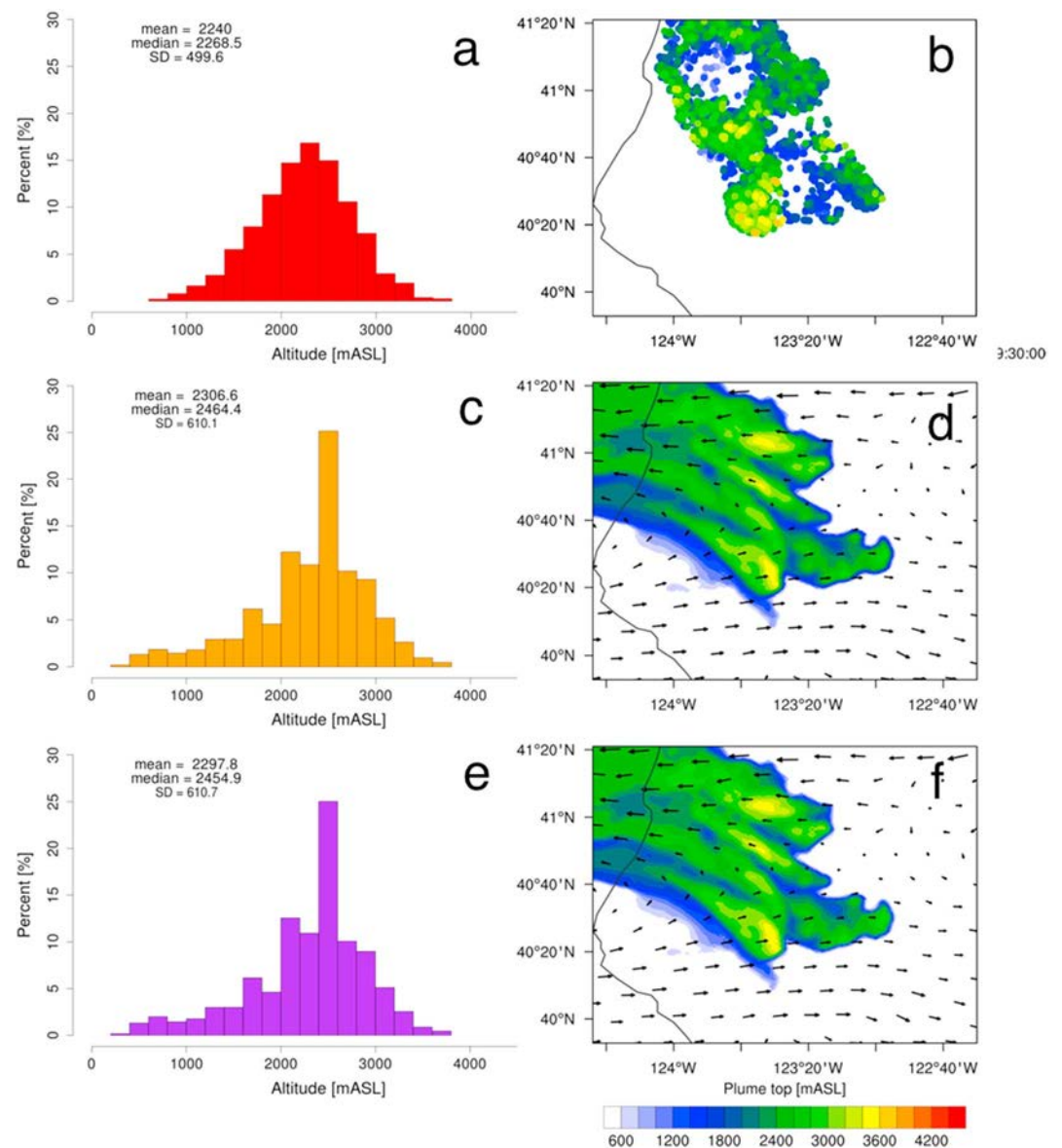


**Figure 7.** MISR observed versus modeled smoke plume tops on 18 August 2015 at 1930 UTC. (left column) Histograms of plume top heights. (right column) Spatial map of the plume top height. (a and b) MISR observations, (c and d) WRFSC hindcast simulation, and (e and f) WRFSC forecast simulation.

between Route and South Complex fires, was significantly overestimated ( $\sim 158\%$ ).  $PM_{2.5}$  at stations 1 and 4 were moderately underestimated by  $-7$  and  $-19\%$ , respectively.

#### 4.2. Sensitivity Analysis Based on the Hindcast Simulations

Model simulations with and without the radiative impact were used to quantify the impacts of smoke aerosols on incoming solar radiation across Northern California between 16 and 23 August 2015. Fires simulated in hindcast mode were constrained using observed fire perimeters, which is discussed in further length in section 2. Unsurprisingly, the baseline simulation, which does not account for the radiative impact of smoke, was unable to capture the reductions of incoming solar radiation at BGBC1 during the afternoon on 19 August (Figure 8a). Here the incoming solar radiation peaked at  $900 \text{ W/m}^2$  during the afternoon, while the observations measured significantly lower values ( $<400 \text{ W/m}^2$ ) during this time. Measurements at TCAC1 station showed a smaller decrease in incoming solar radiation relative to BGBC1, which was also

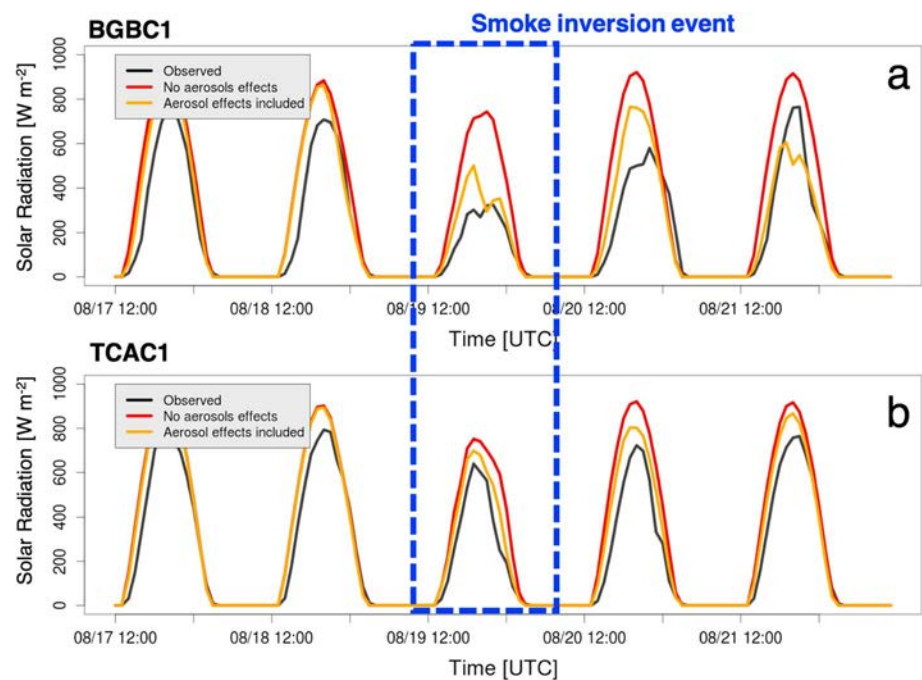


**Figure 8.** Modeled and observed incoming solar radiation at (a) BGBC1 and (b) TCAC1. The red line represents the baseline configuration without aerosol effects and the orange line represents the model configuration with radiatively active smoke.

not captured by the baseline simulation. The baseline simulation also failed to capture differences in the incoming solar radiation between these two locations (Figures 5, 8a, and 8b).

The model configuration that included the radiative effects of smoke aerosols performed significantly better, and reduced the positive bias in the modeled incoming solar radiation at BGBC1 (Figure 8a) on 19 August from over  $400 \text{ W/m}^2$  to less than  $100 \text{ W/m}^2$ . The coupling between the smoke and the radiation scheme was able to resolve the decreases in incoming solar radiation during the afternoon of 19 and 20 August as evident in the time series for BGBC1 and TCAC1 (Figures 8a and 8b). These results suggest that the observed decreases in solar radiation at TCAC1 and BGBC1 were likely associated with the presence of smoke. The thick smoke layer covering the Trinity River Valley likely caused the observed discrepancies between the solar radiation measured at BGBC1 and TCAC1. Here BGBC1 was located deeper in the valley and was covered by a thicker layer of smoke, while TCAC1, which is located at a higher elevation, was covered by a shallower layer of smoke.

The impact of the fire smoke is also evident in the 2-m air temperature time series (Figure 9). Prior to the smoke event, conditions observed during the simulations with and without radiative impacts of smoke were nearly identical. However, during the afternoon of 19 August, temperatures for these simulations showed noticeable differences. While part of the temperature decrease observed at BGBC1 and TCAC1 was likely driven by an approaching shortwave trough breaking down the 500-hPa ridge centered along the Pacific Coast (Figure 6), the WRFSC simulation that accounted for aerosol direct effects showed 2-m temperatures that were  $3^\circ\text{C}$  cooler at BGBC1 relative to the baseline simulation. The time series for the TCAC1 also showed some cooling due to smoke aerosols. However, the cooling at TCAC1 was not nearly as pronounced as the cooling observed at BGBC1.

In order to assess the fire impact on the thermal structure of the atmosphere, vertical temperature profiles over the Trinity Valley were analyzed. The comparison between the baseline simulation and the generic WRF simulation without fire did not reveal any appreciable differences in the temperature profiles within Trinity Valley (not shown). This suggests that the thermal effect of the fires was very localized. From this, it can be hypothesized that for this particular case, the direct thermal effect of the fire did not contribute to the observed inversions. However, differences between the baseline simulation and the WRFSC run with aerosol feedbacks indicate that wildfires smoke had a significant impact on the thermal structure of the

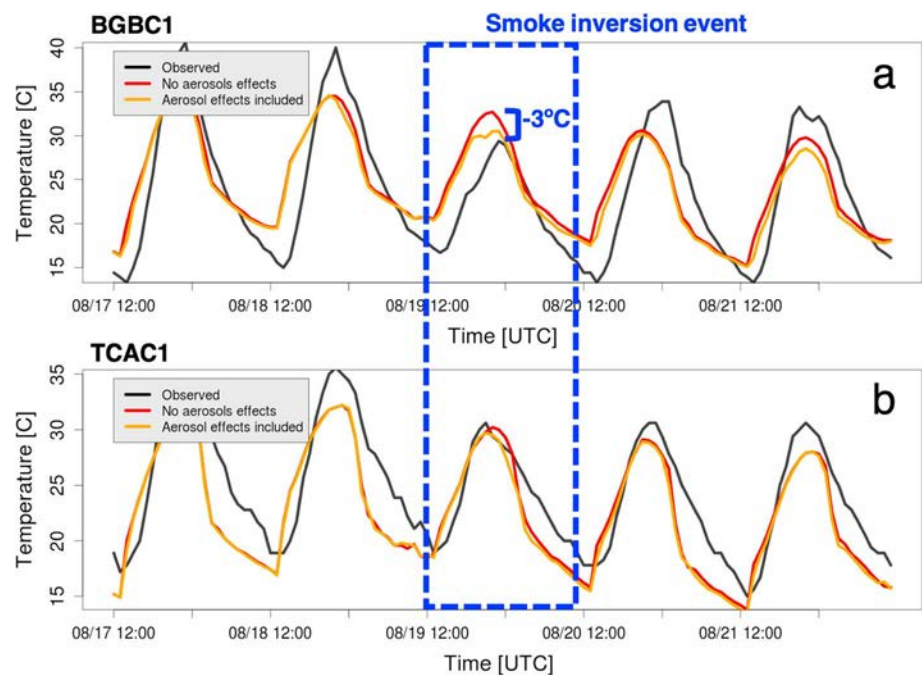


**Figure 9.** Modeled and observed 2-m temperature at (a) BGBC1 and (b) TCAC1. The red line represents the baseline configuration without aerosol effects and the orange line represents the model configuration with radiatively active smoke.

atmosphere (Figure 10). Here smoke shaded the surface, which resulted in low-level cooling, while the absorption of radiation resulted in slight warming aloft ( $+0.5^{\circ}\text{C}$ ). This dual effect stabilized the atmosphere and promoted persistent smoke-enhanced inversions (see Figure 10c).

Model results across Northern California on 19 August at 2100 UTC indicate that much of the area was affected by wildfire-emitted  $\text{PM}_{2.5}$ , with vertically (column) integrated concentrations exceeding  $100 \text{ mg/m}^2$  (Figure 11a). Incoming solar radiation was significantly reduced in the simulation including the aerosol impacts relative to the baseline simulation, with some locations observing decreases approaching  $600 \text{ W/m}^2$  (Figure 11b). Similar decreases were also observed for 2-m temperatures, which were mostly confined to river valleys across Northern California (Figure 11c). Wind speed reductions were also seen across the study region (Figure 11d), which was likely the result of smoke-induced stability reducing vertical mixing and decoupling surface winds from the free troposphere.

The visible correlation between the patterns of column-integrated  $\text{PM}_{2.5}$ , solar radiation reductions, and surface cooling indicates that the observed dampening of the diurnal temperature cycle at BGBC1 was related to the local impacts of the wildfire smoke, which strengthened the inversion by decreasing the amount of incoming solar radiation that reaches the surface, thus reducing surface heating rates and suppressing planetary boundary layer (PBL) growth (Figure 11e). It is suspected that surface cooling associated with smoke shading reduced simulated PBL heights relative to the WRFSC simulation without aerosol-radiative feedback. The regions with large column-integrated  $\text{PM}_{2.5}$  values experienced inhibited PBL growth, with boundary layer heights being reduced by  $\sim 400 \text{ m}$  relative to the baseline simulation. As a result, suppressed PBL growth during the afternoon allowed for near-surface smoke accumulation as seen in Figure 11f. Through the six panels in Figure 11, it can be hypothesized that thick smoke was likely responsible for driving a positive feedback mechanism where smoke shading resulted in increasing stability as a consequence of surface cooling and warming aloft. This effect likely suppressed vertical mixing and PBL growth, reduced near-surface winds, and allowed smoke to accumulate within mountain valleys. A more rigorous analysis was carried out in section 4.4 to confirm this hypothesis.

### 4.3. The Analysis of the Forecast Simulation

In an effort to assess whether the plume rise and radiative smoke effects can be successfully rendered in a fully coupled forecast configuration, results from the forecast simulation were analyzed, similar to the

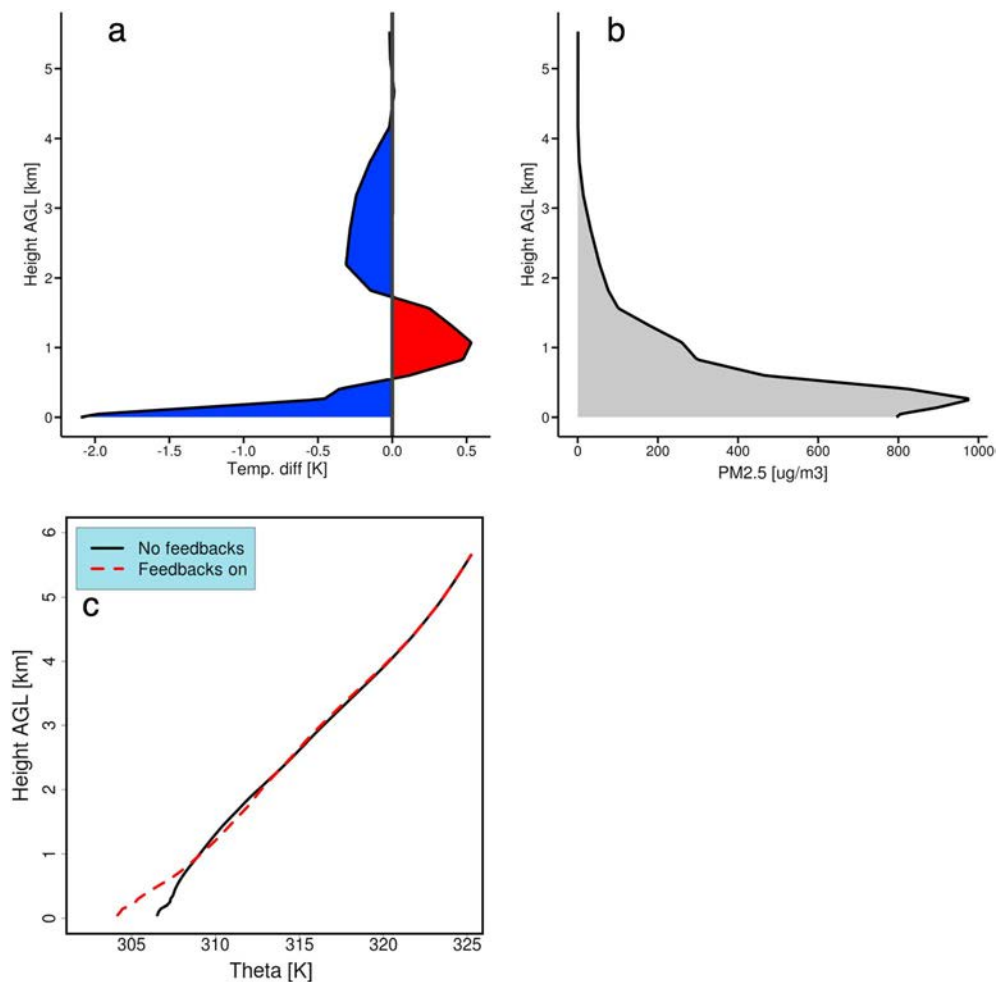


**Figure 10.** (a) Temperature differences between the configuration that included aerosol radiative impacts and the baseline simulation for a location near BGBC1. (b) Simulated vertical PM<sub>2.5</sub> concentrations with radiatively active smoke. (c) Simulated  $\theta$  profiles. Panels are for 19 August 2015 at 1830 UTC.

hindcast run configuration (section 4.2). Plume top heights from this simulation were nearly identical to the run with constrained fire progression. The smoke orientation and the range of plume top height values were comparable to the hindcast simulation (Figures 7d and 7e) while the forecast mean plume top height matched the MISR-derived mean plume top height (2,298 versus 2,240 m). The statistics for the forecasted PM<sub>2.5</sub> concentrations (Table 3) were also comparable to the results from the hindcast run summarized in Table 2. Similar to the hindcast simulation, the highest concentrations simulated in the forecast configuration were also reported at station 3, followed by stations 4, 1, 5, and 2. These results are comparable to the trends observed in the measurements and hindcast simulation. However, relative to the hindcast simulation, the forecast did produce higher concentrations of PM<sub>2.5</sub>. PM<sub>2.5</sub> concentrations at all the sites with the exception of station 1 were overestimated by the forecast simulation, with the highest bias once again occurring at the station 3. Since station 3 is located between the South Complex and Route fires, it is suspected that this site is particularly sensitive to the simulated fire progression. Due to station 3's close proximity to the Route and South Complex fire, even small errors in fire progression could result in significant biases in the simulated smoke concentration.

Next, temperature and incoming solar radiation at TCAC1 and BGBC1 were compared to the observations to verify whether the forecast run was able to capture the smoke-atmosphere interactions observed in the hindcast run. As presented in Figure 12, the simulation with forecasted fire progression was able to reproduce both the reduction of incoming solar radiation in the afternoon of 19 August, in addition to the relative

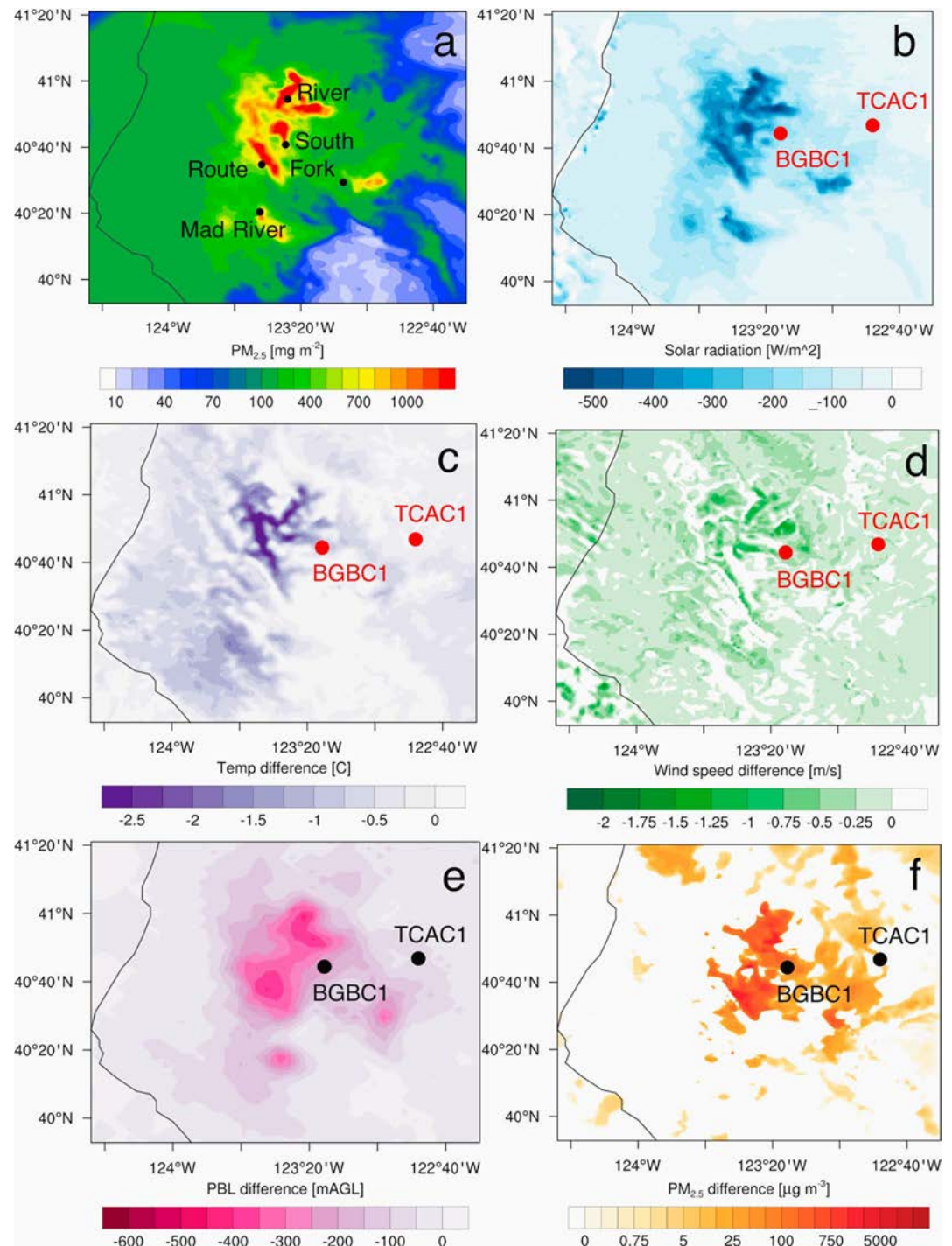


**Figure 11.** (a) Column-integrated  $PM_{2.5}$  concentrations from the model simulation that included radiative aerosol radiative impacts. Fire locations are denoted by black text. Differences between the WRF-SFIRE configuration that included aerosol impacts and the baseline simulations for (b) solar radiation, (c) 2-m temperature, (d) wind speed, (e) PBL height, and (f) surface  $PM_{2.5}$ . Panels are for 19 August 2015 at 1900 UTC.

differences in the smoke shading effects at the BGBC1 and the TCAC1 sites. It is worth noting that the forecast time series of the incoming solar radiation and the 2-m air temperature were very similar to the results from the hindcast run (Figures 12, 8, 13, and 9), with differences less than  $100 \text{ W/m}^2$  and  $1^\circ\text{C}$ , respectively.

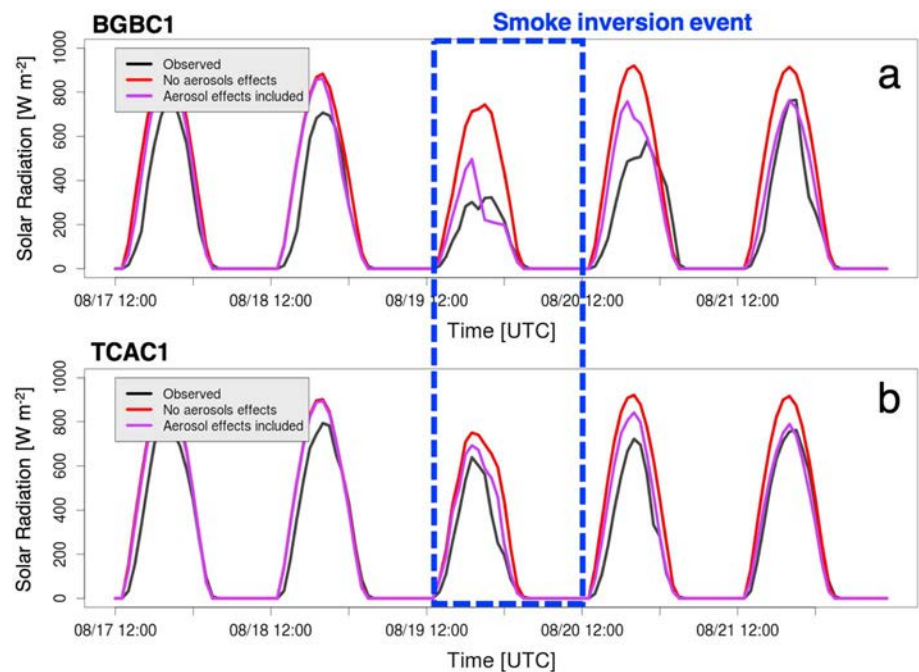


**Figure 12.** Modeled and observed incoming solar radiation at (a) BGBC1 and (b) TCAC1. The red line represents the baseline configuration without aerosol effects and the orange line represents the forecast model run with resolved fire progression and radiatively active smoke.

Finally, differences between the baseline and forecast configuration were computed for incoming solar radiation, 2-m temperature, 10-m winds, PBL heights, and near-surface  $\text{PM}_{2.5}$  concentrations (Figure 14). Similar to the results for the hindcast configuration, the forecast simulation was able replicate the observed

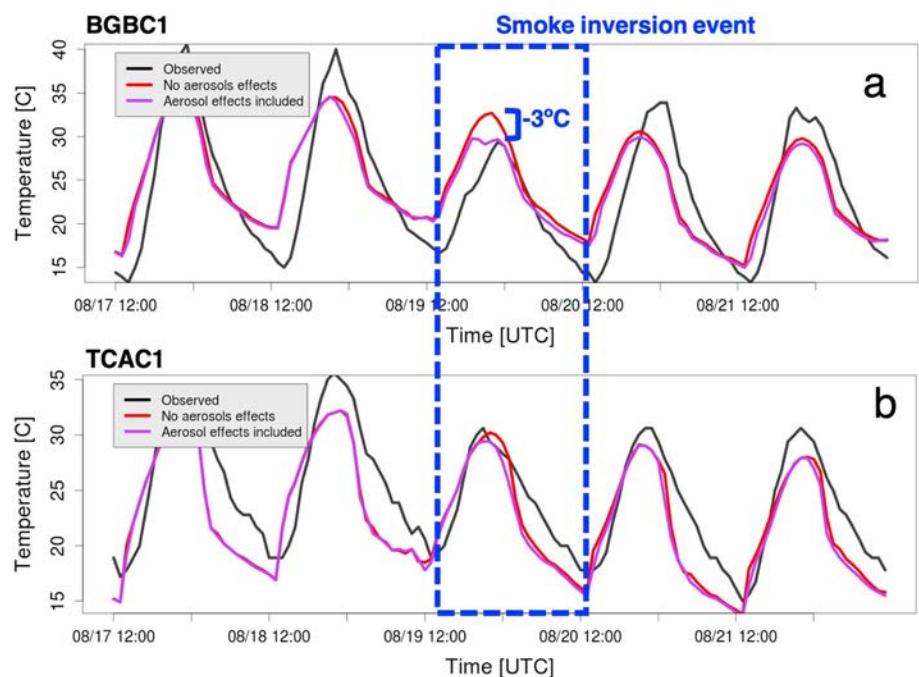


**Figure 13.** Modeled and observed 2-m air temperature at (a) BGBC1 and (b) TCAC1. The red line represents the baseline configuration without aerosol effects and the orange line represents the forecast model run with resolved fire progression and radiatively active smoke.

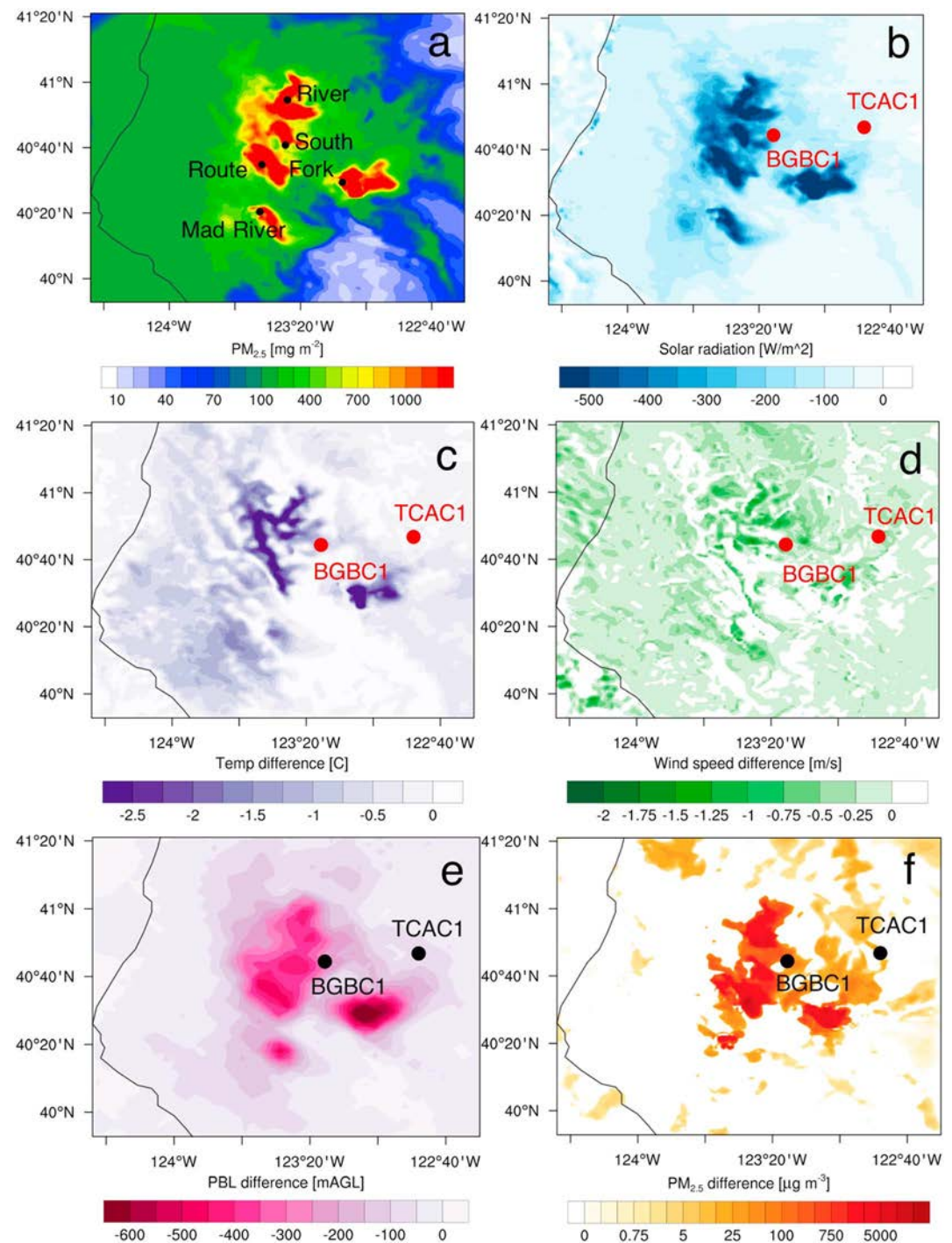


**Figure 14.** (a) Column-integrated  $PM_{2.5}$  concentrations from the forecast model simulation that included aerosol radiative impacts. Fire locations are denoted by black text. Differences between the WRFSC forecast configuration that included aerosol impacts and the baseline simulations for (b) solar radiation, (c) 2-m temperature, (d) wind speed, (e) PBL height, and (f) surface  $PM_{2.5}$ . Panels are for 19 August 2015 at 1900 UTC.

positive feedback mechanism where smoke shading resulted in increased low-level stability, weaker surface winds, lower PBL heights, and weaker smoke dispersion, which translated into smoke accumulation within valleys. These results indicate that even the relatively simple representation of the fire progression based on the semiempirical Rothermel model coupled with the fuel moisture and atmospheric model may be

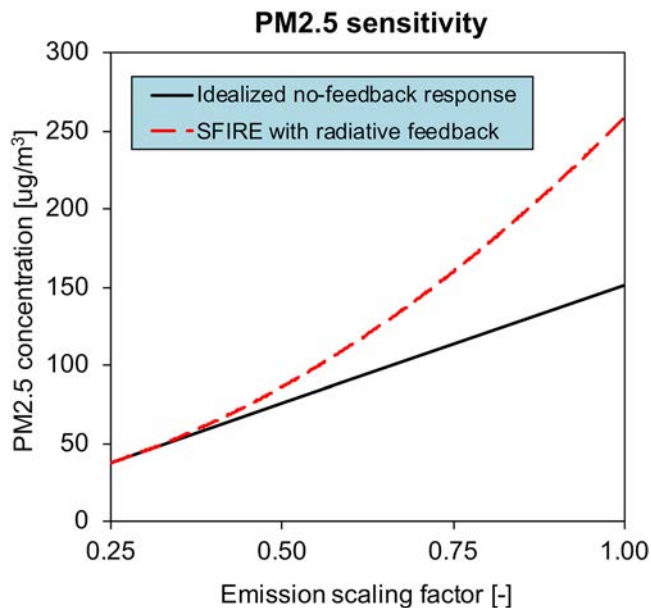


**Figure 15.** Sensitivity of the near-surface  $\text{PM}_{2.5}$  concentration in response to the changes in the smoke emissions showing the effect of radiative feedback. Scaling factor is the fraction of the originally used emission fluxes. The solid black line shows an ideal response without feedback. The dashed red line shows the simulated response with radiative feedback on.

sufficient for forecasting smoke production and smoke-induced inversions within the WRFSC modeling framework.

#### 4.4. Analysis of the Feedback Mechanism

In an effort to verify the positive feedback hypothesis presented in sections 4.2 and 4.3, additional numerical simulations were carried out that focused on the sensitivity of near-surface  $\text{PM}_{2.5}$  concentrations to variations in smoke emissions. These runs, utilizing radiatively active smoke, were executed with the emission fluxes reduced to 25% and 50% of their original values. If positive feedback were not present, the enhancement in the near-surface  $\text{PM}_{2.5}$  concentrations associated with the smoke fluxes should be reduced to 0.25 of their original values, with this decrease being directly proportional to the decrease in emissions. In other words, doubling of the emissions would result in doubling the  $\text{PM}_{2.5}$  concentrations. However, in the case where a positive feedback is present,  $\text{PM}_{2.5}$  should increase more rapidly relative to the changes in the emissions.

The sensitivity of the near-surface  $\text{PM}_{2.5}$  concentrations to changing emissions is shown in Figure 15.  $\text{PM}_{2.5}$  concentrations plotted in Figure 15 represent near-surface conditions within valleys with most persistent and thickest smoke. The values used to construct the red line were computed as averages, across all the points in the domain that experienced a  $>75\%$  enhancement in the surface  $\text{PM}_{2.5}$  concentrations during the afternoon of 19 August as a result of radiative smoke impacts. The enhancements were computed as a difference between the baseline run without

radiative smoke, and the constrained run accounting for radiative smoke effects. The black line Figure 15 shows an ideal no-feedback linear relationship between the concentrations and emissions. The noticeable divergence between the red and the black line indicates the presence of a positive feedback, which resulted in the surface  $\text{PM}_{2.5}$  concentrations that increased at greater rate than the no-feedback linear relationship.

This feedback mechanism was further investigated by analyzing the time evolution of the incoming radiation, the PBL height, and the  $\text{PM}_{2.5}$  concentration in response to a step-type disturbance, which was applied

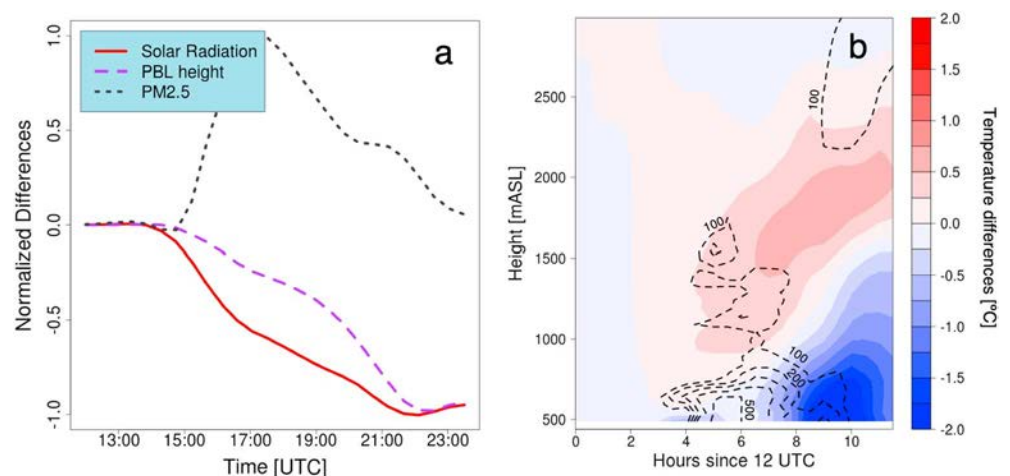


**Figure 16.** (a) Response of the solar radiation (solid red line), PBL height (dashed purple line), and  $\text{PM}_{2.5}$  (black dotted line) to the radiative feedback activated at 1200 UTC. The plotted values represent normalized differences between the run with the feedback instantaneously turned on, and the baseline no-feedback simulation. The maximum magnitudes of differences between solar radiation, PBL, and  $\text{PM}_{2.5}$  are  $350 \text{ W/m}^2$ , 320 m above ground level, and  $560 \mu\text{g/m}^3$ , respectively. (b) Height-time cross section of differences in temperature (color-filled) and  $\text{PM}_{2.5}$  (dashed contour) from the run with feedback turned on, and the baseline no-feedback simulation.  $\text{PM}_{2.5}$  dashed contours include differences starting from  $+100 \mu\text{g/m}^3$  and are contoured every  $100 \mu\text{g/m}^3$ .

as an instantaneous smoke radiative forcing. This analysis was based on a comparison between the baseline no-feedback simulation, and a new run in which the radiative feedback was instantaneously activated on 19 August 1200 UTC, several hours prior the onset of the analyzed smoke episode. The time series presented in Figure 16 shows a notable time shift between the normalized values of the incoming solar radiation, PBL height, and surface concentrations. The plotted values are normalized differences between the run with the feedback instantaneously turned on, and the baseline no-feedback simulation. Reductions in incoming solar radiation appear first at 14:00 UTC (7 am local time), followed by a decrease in PBL heights an hour later. At the same time, there is also an increase in the  $PM_{2.5}$  relative to the simulation with no aerosol radiative feedback. This increase peaks at 1800 UTC (11:00 LST) and starts decreasing as an approaching short-wave trough increases near-surface winds, which starts to erode away the smoke-induced inversion. Figure 16a suggests that the initial response to the presence of the radiative active aerosols is a reduction in the incoming solar radiation and surface cooling, which inhibits mixing, reduces the surface winds, and decreases the PBL height, which in turn increases surface smoke concentrations. When the maximum reduction in the incoming solar radiation reaches  $350 \text{ W/m}^2$ , the PBL heights decrease by 320 m above ground level, while the near-surface  $PM_{2.5}$  concentrations increase by up to  $560 \mu\text{g/m}^3$ .

Vertical time cross sections of differences between the model configurations with and without aerosol feedbacks reveal that weak near-surface cooling at 1600 UTC (9:00 LST) resulted in an increase in  $PM_{2.5}$  45 min later (Figure 16b). Following the rapid increase in  $PM_{2.5}$  concentrations from 1700 to 1800 UTC, temperatures rapidly decreased through the late afternoon. At the same time, warming aloft due to the presence of smoke aerosols further increased stability between 500 and 1,200 m above sea level.

These results are consistent with Yu et al., 2002 who modeled the radiative impact of aerosols on the PBL evolution using a one-dimensional boundary layer model, as well as with Jacobson and Kaufman (2006) who analyzed wind speed reductions due to aerosols over California.

## 5. Conclusions

Observation-based studies have indicated that wildfire smoke can have significant impacts on local meteorology through interactions between wildfire smoke and incoming solar radiation (Lareau & Clements, 2015; Robock, 1988). However, due to the lack of observations, which are needed to fully explain wildfire smoke-atmosphere interactions, the mechanism that drives this interaction remains unclear. As a result, models are often needed to fill in the gaps where observational data are absent or unavailable.

Modeling results presented here confirm that local fire-atmosphere feedback due to the direct effects wildfire smoke can have significant impacts on local weather conditions, which agrees with results from observation-based studies (Lareau & Clements, 2015; Robock, 1988). This study represents the first attempt to resolve the interactions between wildfire smoke and the atmosphere in a fully coupled framework. This work highlights the need for operational NWP models to account for the effects of wildfire smoke, especially for regions susceptible to wildfire activity and smoke-induced inversions, such as mountain valleys across the western United States. In the case study analyzed here, wildfire smoke reduced incoming solar radiation by as much as  $600 \text{ W/m}^2$ , which lead to local surface cooling reaching  $3^\circ\text{C}$  in mountain valleys across Northern California. In addition, model results indicate that smoke aerosols resulted in warming aloft ( $+0.5^\circ\text{C}$ ), which increased atmospheric stability. These results are consistent with a modeling study by Walter et al. (2016), which found that shading from smoke plumes reduced surface temperatures by upward of  $3\text{--}4^\circ\text{C}$ , while absorption from soot increased temperatures aloft by  $0.5\text{--}1^\circ\text{C}$ . It is worth noting that the simulations carried out here excluded the indirect effects (microphysical effects) of smoke aerosols on local meteorology. The microphysical impacts of wildfire smoke will need to be investigated in a future study.

This work suggests that the inclusion of fire-smoke-atmosphere feedback in a coupled modeling framework such as WRFSC may help capture the impacts of wildfire smoke on near-surface stability and local inversions. Furthermore, smoke may have impacts beyond increasing atmospheric stability and decreasing temperatures in smoke-infiltrated valleys. Smoke-enhanced inversions can inhibit the vertical mixing and consequently reduce near-surface winds. This interaction generates a positive feedback, where the smoke layer cools the surface, stabilizes the atmosphere, inhibits the PBL growth, and reduces surface winds, limiting smoke ventilation and promoting persistent inversions. As a result of this feedback, near-surface  $PM_{2.5}$

concentrations build up, particularly in the bottom of mountain valleys. For locations near the fires, increases in  $\text{PM}_{2.5}$  concentrations exceeded  $500 \mu\text{g}/\text{m}^3$ , which can have significant impacts on air quality and visibility. Since most fire management operations are carried out adjacent to wildfires, these results demonstrate the need for NWP models to account for impacts of smoke-induced inversions. Furthermore, these results suggest that a fully coupled fire-atmosphere model that can account for direct aerosol-radiation feedback is needed in order to drive the positive feedback mechanism associated with smoke-enhanced inversions.

While the results here are promising, the simulations presented should only be treated as a proof of concept. Targeted experiments like the Fire and Smoke Evaluation Experiment (Prichard et al., 2019), providing comprehensive description of the fuel characteristics, fire behavior, local meteorology, and emissions, are necessary for validating coupled fire-atmosphere models, as well as assessing their strengths and weaknesses. For example, fire emissions often have significant uncertainties, particularly for radiatively active aerosols such as black and organic carbon due to uncertainties associated with fire emission factors (Urbanski, 2014). As a consequence, all NWP models that simulate fire emissions will have uncertainties associated with smoke. Additional work is also needed to understand the impact of smoke feedback on the fire propagation itself. Smoke-induced inversions may decelerate surface winds. However, inversion breakups or upslope fire propagation that protrudes through the inversion layer could lead to unexpected fire acceleration, which is crucial to understand from a fire safety and air quality perspective.

#### Acknowledgments

This research was sponsored by the USDA grant 16-CS-11132543-075 and NASA grant NNX13AH59G. The authors would like to acknowledge high-performance computing support from Cheyenne (doi:10.5065/D6RX99HX) provided by NCAR's Computational and Information Systems Laboratory, sponsored by the National Science Foundation. The computing support from the University of Utah Center for High Performance Computing is greatly appreciated. The WRFSC model used in this study is available at <http://github.com/openwfm/wrf-fire/>. The output from the presented simulations is available at <https://tinyurl.com/yxqbcjgb>.

#### References

- Achtemeier, G. L. (2009). On the formation and persistence of superfog in woodland smoke. *Meteorological Applications*, 16(2), 215–225. <https://doi.org/10.1002/met.110>
- Ahmadov, R., G. Grell, E. James, S. Freitas, G. Pereira, I. Csiszar, et al. (2017). A high-resolution coupled meteorology-smoke modeling system HRRR-Smoke to simulate air quality over the CONUS domain in real time, Geophysical Research Abstracts Vol. 19, EGU2017-10841, 2017. Retrieved from <http://meetingorganizer.copernicus.org/EGU2017/EGU2017-10841.pdf> (last accessed 02.27.2019).
- Akagi, S. K., Yokelson, R. J., Wiedinmeier, C., Alvarado, M. J., Reid, J. S., Karl, T., et al. (2011). Emission factors for open and domestic biomass burning for use in atmospheric models. *Atmospheric Chemistry and Physics*, 11(9), 4039–4072. <https://doi.org/10.5194/acp-11-4039-2011>
- Chen, S.-H., & Sun, W.-Y. (2002). A one-dimensional time dependent cloud mode. *Journal of the Meteorological Society of Japan*, 80(1), 99–118. <https://doi.org/10.2151/jmsj.80.99>
- Chin, M., Rood, R. B., Lin, S.-J., Muller, J. F., & Thompson, A. M. (2000). Atmospheric sulfur cycle in the global model GOCART: Model description and global properties. *Journal of Geophysical Research*, 105(D20), 24,671–24,687. <https://doi.org/10.1029/2000JD900384>
- Colbeck, I., Atkinson, B., & Johar, Y. (1997). The morphology and optical properties of soot produced by different fuels. *Journal of the Atmospheric Sciences*, 28, 715–723.
- Emmons, L., Walters, S., Hess, P. G., Lamarque, J.-F., Pfister, G. G., Fillmore, D., et al. (2010). Description and evaluation of the Model for Ozone And Related chemical Tracers, version 4 (MOZART-4). *Geoscientific Model Development*, 3(1), 43–67. <https://doi.org/10.5194/gmd-3-43-2010>
- Garrett, J. R., Pittock, A. B., & Walsh, K. (1990). Response of the atmospheric boundary layer and soil layer to high altitude, dense aerosol cover. *Journal of Applied Meteorology*, 29(1), 35–52. [https://doi.org/10.1175/1520-0450\(1990\)029<0035:ROTABL>2.0.CO;2](https://doi.org/10.1175/1520-0450(1990)029<0035:ROTABL>2.0.CO;2)
- Goodrick, S. L., Achtemeier, G. L., Larkin, N. K., Narasimhan, Y. L., & Strand, T. (2012). Modelling smoke transport from wildland fires: A review. *International Journal of Wildland Fire*, 22(1), 83. <https://doi.org/10.1071/WF11116>
- Grell, G., & Baklanov, A. (2011). Integrated modeling for forecasting weather and air quality: A call for fully coupled approaches. *Atmospheric Environment*, 45(38), 6845–6851. <https://doi.org/10.1016/j.atmosenv.2011.01.017>
- Grell, G. A., & Devenyi, D. (2002). A generalized approach to parameterizing convection combining ensemble and data assimilation techniques. *Geophysical Research Letters*, 29(14), 1693. <https://doi.org/10.1029/2002GL015311>
- Hong, S.-Y., Noh, Y., & Dudhia, J. (2006). A new vertical diffusion package with an explicit treatment of entrainment processes. *Monthly Weather Review*, 134(9), 2318–2341. <https://doi.org/10.1175/MWR3199.1>
- Huttunen, K., Siponen, T., Salonen, I., Yli-Tuomi, T., Aurela, M., Dufva, H., et al. (2012). Low-level exposure to ambient particulate matter is associated with systemic inflammation in ischemic heart disease patients. *Environmental Research*, 116, 44–51. <https://doi.org/10.1016/j.envres.2012.04.004>
- Iacono, M. J., Delamere, J. S., Mlawer, E. J., Shephard, M. W., Clough, S. A., & Collins, W. D. (2008). Radiative forcing by long-lived greenhouse gases: Calculations with the AER radiative transfer models. *Journal of Geophysical Research*, 113(D13), D13103. <https://doi.org/10.1029/2008JD009944>
- Ignotti, E., Hacon, S. S., Junger, W. L., Mourão, D., Longo, K., Freitas, S., et al. (2010). Air pollution and hospital admissions for respiratory diseases in the subequatorial Amazon: A time series approach. *Cadernos de Saúde Pública*, 26(4), 747–761. <https://doi.org/10.1590/S0102-311X2010000400017>
- Jacobson, M. Z., & Kaufman, Y. J. (2006). Wind reduction by aerosol particles. *Geophysical Research Letters*, 33, L24814. <https://doi.org/10.1029/2006GL027838>
- Johnston, F. H., Henderson, S. B., Chen, Y., Randerson, J. T., Marlier, M., Defries, R. S., et al. (2012). Estimated global mortality attributable to smoke from landscape fires. *Environmental Health Perspectives*, 120(5), 695–701. <https://doi.org/10.1289/ehp.1104422>
- Kaufman, Y. J., & Nakajima, T. (1993). Effect of Amazon smoke on cloud microphysics and albedo-analysis from satellite imager. *Journal of Applied Meteorology*, 32(4), 729–744. [https://doi.org/10.1175/1520-0450\(1993\)032<0729:EOASOC>2.0.CO;2](https://doi.org/10.1175/1520-0450(1993)032<0729:EOASOC>2.0.CO;2)

- Kochanski, A. K., Jenkins, M. A., Yedinak, K., Mandel, J., Beezley, J., & Lamb, B. (2016). Toward an integrated system for fire, smoke, and air quality simulations. *International Journal of Wildland Fire*, 25(5), 534–568. <https://doi.org/10.1071/wf14074>
- Lareau, N. P., & Clements, C. B. (2015). Cold Smoke: Smoke-induced density currents cause unexpected smoke transport near large wildfires. *Atmospheric Chemistry and Physics*, 15(20), 11,513–11,520. <https://doi.org/10.5194/acp-15-11513-2015>
- Larkin, N. K., O'Neill, S. M., Solomon, R., Raffuse, S., Strand, T., Sullivan, D. C., et al. (2009). The BlueSky smoke modeling framework. *International Journal of Wildland Fire*, 18(8), 906–920. <https://doi.org/10.1071/WF07086>
- Li, Z. Q., Guo, J. P., Ding, A. J., Liao, H., Liu, J. J., Sun, Y. L., et al. (2017). Aerosol and boundary-layer interactions and impact on air quality. *National Science Review*, 4(6), 810–833. <https://doi.org/10.1093/nsr/nwx117>
- Liu, Y., Achtemeier, G., & Goodrick, S. (2008). Sensitivity of air quality simulation to smoke plume rise. *Journal of Applied Remote Sensing*, 2(1), 021503. <https://doi.org/10.1117/1.2938723>
- Mallia, D. V., Kochanski, A. K., Urbanski, S. P., & Lin, J. C. (2018). Optimizing smoke plume rise modeling approaches at local scales. *Atmosphere*, 9(5), 166. <https://doi.org/10.3390/atmos9050166>
- Mandel, J., Beezley, J. D., & Kochanski, A. K. (2011). Coupled atmosphere-wildland fire modeling with WRF 3.3 and SFIRE 2011. *Geoscientific Model Development*, 4(3), 591–610. <https://doi.org/10.5194/gmd-4-591-2011>
- Nelson, D., Averill, C., Boland, S., Morford, R., Garay, M., Thompson, C., et al. (2008). *MISR Interactive eXplorer (MINX) v1.0 user's guide*. Washington, DC: Published on the web: Jet Propulsion Lab, NASA. <https://www.openchannelsoftware.com/projects/MINX>
- Nelson, D., Chen, Y., Kahn, R., Diner, D., & Mazzoni, D. (2008). Example applications of the MISR INteractive eXplorer (MINX) software tool to wildfire smoke plume analyses. In W. M. Hao (Ed.), *Remote sensing of fire: Science and application, Proc SPIE*, 7089. <https://doi.org/10.1117/12.795087>
- Nelson, D. L., Garay, M. J., Kahn, R. A., & Dunst, B. A. (2013). Stereoscopic height and wind retrievals for aerosol plumes with the MISR Interactive eXplorer (MINX). *Remote Sensing*, 5(9), 4593–4628. <https://doi.org/10.3390/rs5094593>
- Prichard, S., Larkin, N. S., Ottmar, R., French, N. H., Baker, K., Brown, T., et al. (2019). The Fire and Smoke Model Evaluation Experiment —A plan for integrated, large fire-atmosphere field campaigns. *Atmosphere*, 10(2), 66. <https://doi.org/10.3390/atmos10020066>
- Robock, A. (1988). Enhancement of surface cooling due to forest fire smoke. *Science*, 242(4880), 911–913. <https://doi.org/10.1126/science.242.4880.911>
- Robock, A. (1991). Surface cooling due to forest fire smoke. *Journal of Geophysical Research*, 96(D11), 20869. <https://doi.org/10.1029/91jd02043>
- Saha, S., Moorthi, S., Wu, X., Wang, J., Nadiga, S., Tripp, P., et al. (2014). The NCEP Climate Forecast System version 2. *Journal of Climate*, 27(6), 2185–2208. <https://doi.org/10.1175/JCLI-D-12-00823.1>
- Segal, M., Weaver, J. F., & Purdom, J. F. W. (1989). Some effects of the Yellowstone Fire smoke plume on Northeast Colorado at the end of summer 1988. *Monthly Weather Review*, 117(10), 2278–2284. [https://doi.org/10.1175/1520-0493\(1989\)117<2278:SEOTYF>2.0.CO;2](https://doi.org/10.1175/1520-0493(1989)117<2278:SEOTYF>2.0.CO;2)
- Spracklen, D. V., Mickley, L. J., Logan, J. A., Hudman, R. C., Yevich, R., Flannigan, M. D., & Westerling, A. L. (2009). Impacts of climate change from 2000 to 2050 on wildfire activity and carbonaceous aerosol concentrations in the western United States. *Journal of Geophysical Research*, 114(D20), D20301. <https://doi.org/10.1029/2008JD010966>
- Stockwell, W. R., Middleton, P., Chang, J. S., & Tang, X. (1990). The second generation regional acid deposition model chemical mechanism for regional air quality modeling. *Journal of Geophysical Research*, 95(D10), 16,343–16,367. <https://doi.org/10.1029/JD095iD10p16343>
- Stone, R. S., Augustine, J. A., Dutton, E. G., O'Neill, N. T., & Saha, A. (2011). Empirical determinations of the longwave and shortwave radiative forcing efficiencies of wildfire smoke. *Journal of Geophysical Research*, 116(D12), D12207. <https://doi.org/10.1029/2010JD015471>
- Tewari, M., F. Chen, W. Wang, J. Dudhia, M. A. LeMone, K. Mitchell, et al. (2004). Implementation and verification of the unified NOAA land surface model in the WRF model. 20th conference on weather analysis and forecasting/16th conference on numerical weather prediction, pp. 11–15.
- Urbanski, S. (2014). Wildland fire emissions, carbon, and climate: Emission factors. *Forest Ecology and Management*, 317, 51–60. <https://doi.org/10.1016/j.foreco.2013.05.045>
- Val Martin, M., Kahn, R. A., Logan, J. A., Paugam, R., Wooster, M., & Ichoku, C. (2012). Space-based observational constraints for 1-D fire smoke plume-rise models. *Journal of Geophysical Research*, 117.
- Vejmelka M., Kochanski A., & Mandel J. (2015). Data assimilation of dead fuel moisture observations from remote automated weather stations. *International Journal of Wildland Fire*, 25, 558–568. <https://doi.org/10.1071/WF14085>
- Walter, C., Freitas, S. R., Kottmeier, C., Kraut, I., Rieger, D., Vogel, H., & Vogel, B. (2016). The importance of plume rise on the concentrations and atmospheric impacts of biomass burning aerosol. *Atmospheric Chemistry and Physics*, 16(14), 9201–9219. <https://doi.org/10.5194/acp-16-9201-2016>
- Youn, D., Park, R. J., Jeong, J. I., Moon, B.-K., Yeh, S.-W., Kim, Y. H., et al. (2011). Impacts of aerosols on regional meteorology due to Siberian forest fires in May 2003. *Atmospheric Environment*, 45(7), 1407–1412. <https://doi.org/10.1016/j.atmosenv.2010.12.028>
- Yu, H., Liu, S. C., & Dickinson, R. E. (2002). Radiative effects of aerosols on the evolution of the atmospheric boundary layer. *Journal of Geophysical Research*, 107(D12). <https://doi.org/10.1029/2001JD000754>
- Yu, P., Toon, O. B., Bardeen, C. G., Bucholtz, A., Rosenlof, K. H., Saide, P. E., et al. (2016). Surface dimming by the 2013 Rim Fire simulated by a sectional aerosol model. *Journal of Geophysical Research: Atmospheres*, 121, 7079–7087. <https://doi.org/10.1002/2015JD024702>
- Zelikoff, J. T., Chen, L. C., Cohen, M. D., & Schlesinger, R. B. (2002). The toxicology of inhaled wood smoke. *Journal of Toxicology and Environmental Health*, 5(3), 269–282. <https://doi.org/10.1080/10937400290070062>